

An XMM-Newton view of the Symbiotic Stars HM Sge, NQ Gem, and PU Vul

JESÚS A. TOALÁ (杜宇君),¹ MARISSA K. BOTELLO,² AND LAURENCE SABIN²

¹*Instituto de Radioastronomía y Astrofísica, UNAM, Ant. carretera a Pátzcuaro 8701, Ex-Hda. San José de la Huerta, 58089 Morelia, Mich., Mexico*

²*Instituto de Astronomía, Universidad Nacional Autónoma de México, Apdo. Postal 877, 22860 Ensenada, B.C., Mexico*

(Received March 22, 2023)

Accepted to ApJ

ABSTRACT

We present the analysis of archival XMM-Newton observations of the symbiotic stars HM Sge, NQ Gem, and PU Vul. The EPIC-pn spectra hint at the presence of emission lines, which are further confirmed in the 1st order RGS spectra of the three sources. Spectral modeling of the EPIC-pn data disclose unprecedented characteristics, for instance, the best fit to the EPIC-pn spectrum of the β -type symbiotic star PU Vul reveals the presence of two plasma components. We report the discovery of an extremely soft spectral component in the EPIC-pn spectrum of the β -type symbiotic star HM Sge which we suggest is produced by periodic mass ejections such as jets. Consequently, we suggest that a simple β -type classification no longer applies to HM Sge. Finally, the spectrum of the β/δ -type symbiotic star NQ Gem can not be fitted by a two-temperature plasma model as performed by previous authors. The model requires extra components to fit the 1.0–4.0 keV energy range. More sophisticated models to β/δ -type symbiotic stars are needed in order to peer into the accretion process from such systems.

Keywords: Symbiotic binary stars (1674); Stellar accretion(1578); White dwarf stars(1799); X-ray stars; Low mass stars(2050)

1. INTRODUCTION

Symbiotic stars are binary systems composed of a compact object accreting enough material from a red giant to produce observable emission at any wavelength. This definition, proposed by Luna et al. (2013), is intended to be as free as possible from observational selection biases. The definition is somewhat loose if one recognizes that the compact object might be a white dwarf (WD), a neutron star, or even a black hole (see Luna et al. 2013). For this, symbiotic systems have been divided into WD symbiotics and symbiotic X-ray binaries (see for example Chakrabarty & Roche 1997; Enoto et al. 2014; Hinkle et al. 2019). In this paper, we will refer to WD symbiotics simply as symbiotic stars.

In symbiotic stars the WD accretes material from the red giant companion, but it is currently not clear whether the WD accretes material through a Bondi-Hoyle process (Bondi & Hoyle 1944), by Roche-lobe overflow, or a hybrid wind Roche-lobe overflow channel (see Podsiadlowski & Mo-

hamed 2007). Nevertheless, an accretion disk forms surrounding the compact object.

X-ray observations have been classically used to assess the accretion process in WD symbiotic stars, but not many have been detected in X-rays. There are less than 300 confirmed galactic WD symbiotic stars reported in the New Online Database of Symbiotic Variables by 2023 January 30¹ (see also Akras et al. 2019; Merc et al. 2019a), but Merc et al. (2019b) reported that only about 60 have been detected with X-ray instruments. Merc et al. (2019b) suggested that the production of X-ray emission from symbiotic stars should be a common feature, but thus far, the X-ray detections mostly correlate with the brightest and closer systems.

The production of X-rays from symbiotic stars can be attributed to different origins (see Mukai 2017, and references therein). Extremely soft X-rays ($E < 0.5$ keV) can be produced by nuclear burning at the surface of the WD. X-rays are also produced when the accreted material hits the surface of the WD (see the early work of Aizu 1973), but details depend whether the WD is magnetically active or not. In addi-

Corresponding author: Jesús A. Toalá
j.toala@ira.unam.mx

¹ <http://astronomy.science.upjs.sk/symbiotics/>

Table 1. XMM-Newton observations of the three symbiotic stars analyzed here. All observations were obtained with the full-frame mode and the medium optical blocking filter.

Revolution	Obs. ID.	Object	Observation start (UTC)	Observation end (UTC)	Total exposure time			Useful exposure time		
					pn (ks)	MOS1 (ks)	MOS2 (ks)	pn (ks)	MOS1 (ks)	MOS2 (ks)
2725	0740610101	NQ Gem	2014-10-26T12:35:57	2014-10-27T06:17:37	60.75	62.35	62.32	44.80	57.72	56.35
3010	0784910101	PU Vul	2016-05-16T20:56:34	2016-05-17T15:14:54	62.21	60.66	60.64	24.69	41.68	36.55
3078	0784910201	HM Sge	2016-09-29T16:51:07	2016-09-29T20:27:47	10.04	11.65	11.63	7.76	11.20	10.58

tion, outflows originated by the central engine can also produce shocks that heat up the material up to X-ray-emitting temperatures. Strong shocks can be produced either by the fast wind from the WD component or jet-like ejections, both interacting with the slower wind from the cooler companion. High-quality images and spectra are most needed in order to put into context this phenomenology in symbiotic stars (see, e.g., Karovska et al. 2010).

The first X-ray classification of symbiotic stars was presented by Mürset et al. (1997) dividing these objects into three different groups depending on their spectra properties. α -type symbiotic stars corresponds to those sources with super soft X-ray spectra peaking at energies bellow 0.4 keV and attributed to the quasi-steady thermonuclear burning on the surface of the WD (see Orio et al. 2007). β -type objects with spectral peaks close to 0.8 keV are associated with optically-thin plasma with temperatures $\sim 10^6$ K produced by colliding winds, accretion shocks and/or accretion disk. Finally, γ -type corresponds to harder X-ray sources with emission associated with shocks between the accretion material of the compact object that reaches up to 2.4 keV energy. We note that this classification scheme was defined by using ROSAT data which was sensitive to the soft X-ray emission in the 0.1–2.5 keV energy range.

However, given that some symbiotic stars were discovered to emit X-rays with energies above 20 keV (e.g., Chernyakova et al. 2005; Kennea et al. 2009), the original classification scheme proposed by Mürset et al. (1997) had to be revised. Luna et al. (2013) expanded the $\alpha/\beta/\gamma$ classification scheme by adding a fourth category, δ -type for highly absorbed, hard X-ray emission sources. These authors used Swift XRT observations from symbiotic stars covering the 0.4–10 keV energy range. In particular, the X-ray emission from these sources is typically highly extinguished and very likely corresponds to emission from the innermost accretion region surrounding the WD component. Luna et al. (2013) demonstrated that symbiotic stars not only emit soft X-rays, but there was a significant population of objects with hard X-ray emission.

In this work we analyze publicly available, unpublished XMM-Newton observations of the symbiotic stars HM Sge, NQ Gem, and PU Vul which have been classified as β -, β/δ -, and β -type, respectively (see Merc et al. 2019b, and ref-

erences therein). We note that HM Sge and PU Vul have not been studied since the work of Mürset et al. (1997) but NQ Gem is one of the symbiotic stars demonstrated to be part of the β/δ -type using Swift data by Luna et al. (2013). The analysis of the XMM-Newton data presented here improves previous spectral characterization of these three symbiotic stars. This paper is organized as follows. In Section 2 we present the observations and their preparation. Section 3 presents our results and their discussion. Finally, in Sections 4 we list our conclusions.

2. OBSERVATIONS AND DATA PREPARATION

HM Sge, NQ Gem, and PU Vul were observed by XMM-Newton with the European Photon Imaging Cameras (EPIC) on different seasons. In Table 1 we list the details of each observation set. The observations data files were obtained from the XMM-Newton Science Archive². In all cases the three EPIC cameras (pn, MOS1, and MOS2) were used in the full-frame mode with the medium optical blocking filter. The total observing times for HM Sge, NQ Gem, and PU Vul are 13.0, 63.7, and 65.0, respectively. The data were processed with the Science Analysis Software (SAS, version 20.0; Gabriel et al. 2004) with the calibration files obtained on 2022 August 19.

Bad periods characterized by high-background levels were evaluated by analyzing EPIC light curves extracted in the 10.0–12.0 keV energy range. Typical values of 0.5 and 0.2 counts s^{-1} were set as maxima for the pn and MOS cameras, respectively. After cleaning the data, we extracted pn, MOS1, and MOS2 spectra for the three symbiotic stars using the SAS task *evselect* adopting circular apertures centered on each source with radii of $20''$. For the MOS observations events with CCD patterns 0–12 were selected, but for the EPIC-pn data, only events with CCD pattern 0 (single pixel events) were selected. The background spectra were extracted using adjacent regions with no contribution from the symbiotic star or any other source. The calibration matrices were produced with the *rmfgen* and *arfgen* SAS tasks. The resultant background-subtracted spectra of the three symbiotic stars are presented in Fig. 1.

² <http://nxsas.esac.esa.int/nxsas-web/#search>

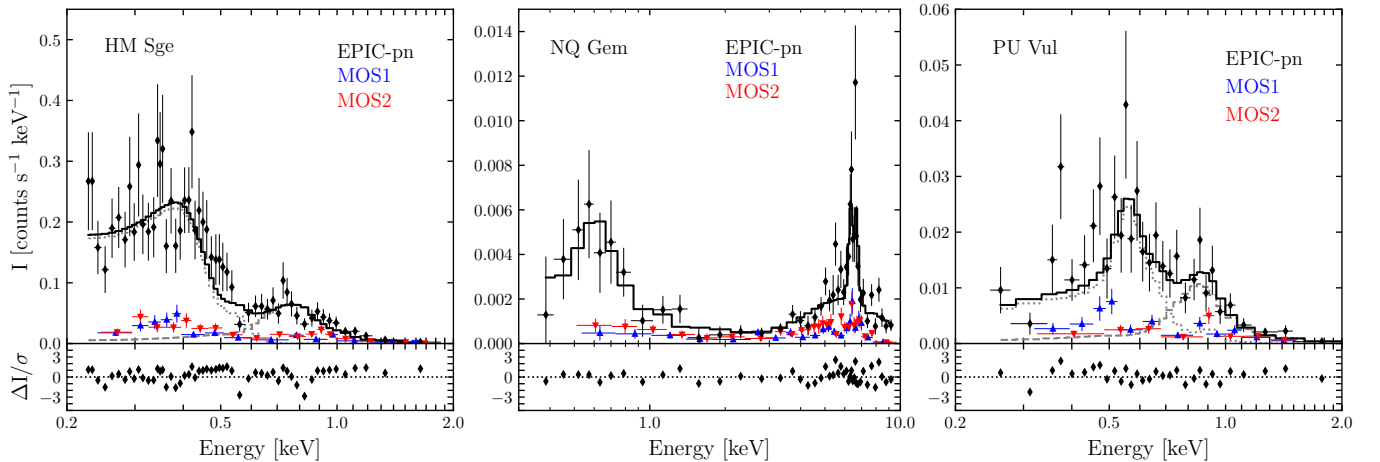


Figure 1. Background-subtracted XMM-Newton EPIC spectra of HM Sge (left), NQ Gem (middle), and PU Vul (right). Colored symbols correspond to the observed spectra while the black histograms represent the best-fit models to the EPIC-pn data. The (gray) dotted and (dashed) lines in the HM Sge and PU Vul panels represent the two different plasma components of their best fit models described in Table 2. In all cases the bottom panels show the residuals.

In addition, we also processed the Reflection Grating Spectrometers (RGS) data also on board XMM-Newton. Although the quality of the RGS spectra hampers a more comprehensive analysis, these were inspected to search for the presence of emission lines which helped us achieve a better interpretation of the EPIC spectra. Some details of the analysis of RGS data as well as the resultant spectra are presented in Appendix A.

The EPIC spectra were modeled with the X-Ray Spectral Fitting Package (XSPEC; version 12.12.1; Arnaud 1996). Extinction of X-rays caused by the interstellar medium (ISM) was included by adopting the Tuebingen-Boulder absorption model *tbabs* (Wilms et al. 2000) which takes into account the absorption produced by the gas-phase ISM, the grain-phase ISM, and the molecules in the ISM³. The hydrogen absorption column densities (N_{H}) for the three symbiotic stars analyzed here were fixed to the values reported by the NASA’s HEASARC N_{H} column density tool (HI4PI Collaboration et al. 2016; Kalberla et al. 2005; Dickey & Lockman 1990)⁴. We adopted the distances estimated by Bailer-Jones et al. (2021) using Gaia data (see Table 2).

In order to fit the EPIC spectra of the three symbiotic stars, we used different model components or a combination of them. Given that symbiotic stars emit X-rays through thermal processes (see Mukai 2017) most of our spectral fits were performed adopting optically-thin collisionally-ionized emission plasma models. In this paper we use the *apec* emission spectrum⁵ included in XSPEC. In all cases we adopted the solar abundances from Lodders et al. (2009). We were

able to extract spectra from the three EPIC cameras (pn, MOS1, and MOS2) as illustrated in Fig. 1. All EPIC spectra were inspected, but the EPIC-pn spectra have superior count rates than those extracted from the MOS instruments. Thus, the spectral modeling will be only performed for those spectra. Nevertheless, we note that the analysis of the MOS spectra result in similar models as those obtained from the EPIC-pn spectra.

Two-temperature plasma components were sufficient to produce good fits to the X-ray emission from HM Sge and PU Vul, but a more complex model was needed for NQ Gem (see Luna et al. 2013). The goodness of the model fits was assessed by the reduced chi squared statistics (χ^2_{DoF}), defined as the χ^2 statistics per degree of freedom (DoF). These values are provided in XSPEC and are also listed in Table 2 for each source.

3. RESULTS AND DISCUSSION

The analysis of the EPIC-pn spectra of HM Sge, NQ Gem, and PU Vul resulted in different models with different implications. Consequently, we will present their results and discussion in separate subsections. Details of the best models are listed in Table 2.

3.1. HM Sge

The EPIC-pn spectrum of HM Sge displays the obvious contribution from two components (see Fig. 1 left panel). One dominating at energies below $E < 0.5$ keV and a secondary contributing at $E > 0.5$ keV. No significant emission is detected beyond 2.0 keV.

The spectrum suggest at the presence of emission lines. The soft ($E < 0.5$ keV) spectral region exhibits apparent peaks at 0.4, 0.3, and 0.2 keV with some emission in the 0.3–0.4 keV range. An additional peak is located at about

³ See further details in <https://heasarc.gsfc.nasa.gov/xanadu/xspec/manual/node268.html>

⁴ <https://heasarc.gsfc.nasa.gov/cgi-bin/Tools/w3nh/w3nh.pl>

⁵ <https://heasarc.gsfc.nasa.gov/xanadu/xspec/manual/XSmodelApec.html>

Table 2. Model parameters of the best fits to the EPIC-pn spectra. The net time (t_{net}), count rate, and total number of counts correspond to the EPIC-pn data of each source. f_X and F_X are the observed and intrinsic fluxes, respectively, whilst L_X is the luminosity.

	HM Sge	NQ Gem	PU Vul
d [kpc]	1.0	1.04	4.1
t_{net} [ks]	7.8	44.8	24.7
Count rate [cnts s $^{-1}$]	8.97×10^{-2}	1.65×10^{-2}	1.22×10^{-2}
Total counts [cnts]	700	740	300
Energy range [keV]	0.2–2.0	0.3–9.0	0.2–2.0
χ^2_{DoF}	62.31/51=1.21	36.20/32=1.13	32.99/26=1.27
$N_{\text{H},1}$ [10^{21} cm $^{-2}$]	3.0	0.49	1.7
kT_1 [keV]	$(2.9^{+0.2}_{-0.2}) \times 10^{-2}$	$0.22^{+0.03}_{-0.03}$	$0.15^{+0.04}_{-0.03}$
A_1 [cm $^{-5}$]	122	$(2.6 \pm 0.8) \times 10^{-6}$	$(3.6 \pm 0.9) \times 10^{-5}$
f_1 [erg cm $^{-2}$ s $^{-1}$]	$(9.8 \pm 3.4) \times 10^{-14}$	$(2.9 \pm 1.1) \times 10^{-15}$	$(9.3 \pm 2.1) \times 10^{-15}$
F_1 [erg cm $^{-2}$ s $^{-1}$]	$(5.3 \pm 1.9) \times 10^{-10}$	$(4.0 \pm 1.9) \times 10^{-15}$	$(6.8 \pm 1.6) \times 10^{-14}$
L_1 [erg s $^{-1}$]	$(6.3 \pm 2.2) \times 10^{34}$	$(5.2 \pm 2.6) \times 10^{29}$	$(1.4 \pm 0.3) \times 10^{32}$
kT_2 [keV]	$0.31^{+0.07}_{-0.04}$	$2.5^{+3.0}_{-2.0}$	$0.75^{+0.29}_{-0.16}$
A_2 [cm $^{-5}$]	8.2×10^{-5}	$(3.0 \pm 0.3) \times 10^{-6}$	$(5.1 \pm 0.9) \times 10^{-6}$
f_2 [erg cm $^{-2}$ s $^{-1}$]	$(4.4 \pm 0.8) \times 10^{-14}$	$(3.1 \pm 1.3) \times 10^{-15}$	$(7.6 \pm 1.3) \times 10^{-15}$
F_2 [erg cm $^{-2}$ s $^{-1}$]	$(1.7 \pm 0.3) \times 10^{-13}$	$(3.5 \pm 1.4) \times 10^{-15}$	$(1.3 \pm 0.2) \times 10^{-14}$
L_2 [erg s $^{-1}$]	$(2.0 \pm 0.4) \times 10^{31}$	$(4.5 \pm 1.8) \times 10^{29}$	$(2.6 \pm 0.5) \times 10^{31}$
Γ	...	-1.5 ± 0.5	...
A_{pow} [cm $^{-5}$]	...	$(1.2 \pm 1.4) \times 10^{-7}$...
f_{pow} [erg cm $^{-2}$ s $^{-1}$]	...	$(1.2 \pm 0.1) \times 10^{-13}$...
F_{pow} [erg cm $^{-2}$ s $^{-1}$]	...	$(1.2 \pm 0.1) \times 10^{-13}$...
L_{pow} [erg s $^{-1}$]	...	$(1.5 \pm 0.2) \times 10^{31}$...
$N_{\text{H},2}$ [10^{21} cm $^{-2}$]	...	390 ± 170	...
kT_3 [keV]	...	4.5 ± 2.0	...
A_3 [cm $^{-5}$]	...	$(4.8 \pm 1.1) \times 10^{-4}$...
f_3 [erg cm $^{-2}$ s $^{-1}$]	...	$(1.1 \pm 0.2) \times 10^{-13}$...
F_3 [erg cm $^{-2}$ s $^{-1}$]	...	$(1.1 \pm 0.2) \times 10^{-13}$...
L_3 [erg s $^{-1}$]	...	$(1.4 \pm 0.3) \times 10^{31}$...
E_{line} [keV]	...	6.4 ± 0.1	...
σ_{line} [keV]	...	$(1.1 \pm 0.1) \times 10^{-1}$...
A_{line} [cm $^{-5}$]	...	$(5.6 \pm 1.3) \times 10^{-6}$...
f_{line} [erg cm $^{-2}$ s $^{-1}$]	...	$(2.8 \pm 0.5) \times 10^{-14}$...
F_{line} [erg cm $^{-2}$ s $^{-1}$]	...	$(2.8 \pm 0.5) \times 10^{-14}$...
L_{line} [erg s $^{-1}$]	...	$(3.6 \pm 0.6) \times 10^{30}$...
f_X [erg cm $^{-2}$ s $^{-1}$]	$(1.4 \pm 0.5) \times 10^{-13}$	$(2.7 \pm 0.5) \times 10^{-13}$	$(1.7 \pm 0.4) \times 10^{-14}$
F_X [erg cm $^{-2}$ s $^{-1}$]	$(5.3 \pm 2.1) \times 10^{-10}$	$(1.0 \pm 0.2) \times 10^{-12}$	$(8.2 \pm 1.8) \times 10^{-14}$
L_X [erg s $^{-1}$]	$(6.3 \pm 2.5) \times 10^{34}$	$(1.3 \pm 0.3) \times 10^{32}$	$(1.6 \pm 0.4) \times 10^{32}$

$\gtrsim 0.7$ keV. Given the low spectral resolution of the EPIC-pn spectra, the presence of emission lines might be questionable. However, the inspection of the 1st order RGS(1+2) spectrum of HM Sge reveals the presence of several emission lines (see the top panel of Fig. A1 in Appendix A). The most prominent lines are those of S XI 31.05, 31.48 Å (~ 0.4 keV), S XII 32.4 Å (~ 0.38 keV) and the unresolved N V triplet at ~ 29.0 Å (~ 0.43 keV). The presence of the C V 35.0 Å (~ 0.35 keV), N V 24.78 Å (0.5 keV) and an unresolved contribution from the O V 18.67 Å and O VI 18.97 Å (~ 0.65 keV) can also be hinted in the spectrum.

Single-temperature plasma models were first attempted, but did not result in acceptable fits ($\chi_{\text{DoF}}^2 > 4$). At best, these models only fit the spectrum for $E < 0.5$ keV. The best model to the EPIC-pn spectrum of HM Sge ($\chi_{\text{DoF}}^2 = 62.31/51 = 1.21$) resulted in two-plasma components with temperatures of $kT_1 = 2.9 \times 10^{-2}$ keV ($= 3.4 \times 10^5$ K) and $kT_2 = 0.31$ keV ($= 3.6 \times 10^6$ K). The total intrinsic X-ray flux and luminosity for the 0.2–2.0 keV energy range are $F_X = (5.3 \pm 2.1) \times 10^{-10}$ erg cm $^{-2}$ s $^{-1}$ and $L_X = (6.3 \pm 2.5) \times 10^{34}$ erg s $^{-1}$, respectively. The detection of the hotter component is consistent with the analysis of the ROSAT PSPC observations presented in Mürset et al. (1997). However, the softer component was not detected in those ROSAT data even though the PSPC instrument had a higher sensitivity towards the soft energy range. We can only suggest that this emission has been enhanced in the recent years.

The extreme soft emission from symbiotic stars ($E < 0.4$ keV) is usually attributed to the quasi-steady thermonuclear burning on the surface of the WD (Orio et al. 2007). However, in the case of HM Sge it could be also explained by the presence of jets. In fact, Corradi et al. (1999) presented optical images to unveiled the presence of jet-like features at distances $\lesssim 8''$ from HM Sge. In addition, their optical spectra suggest deprojected jet velocities of ~ 100 km s $^{-1}$. Assuming an adiabatic shock, the plasma temperature of 3.4×10^5 K suggests a shock velocity of $v_{\text{shock}} \approx 120 \mu^{-1/2}$ km s $^{-1}$, where μ is the mean molecular weight of the particles. The latter is consistent with the estimated jet velocities. In addition, Goldman et al. (2022) presented evidence that HM Sge has been dimming in the past recent years which they attribute to a change in the system orientation or to a sudden mass ejection.

It is interesting to note that the velocity of the jet in HM Sge is at least an order of magnitude below the estimated escape velocity defined by a WD. Bipolar ejections can be produced by thermonuclear runaways at the surface of the WD (see for example the case of the symbiotic recurrent nova RS Oph; Montez et al. 2022), but the situation in this source might be different. Aguayo-Ortiz et al. (2019) presented their *choked accretion* model where they explore the accretion of axi-symmetric, large-scale, small-amplitude in the density structures onto a gravitating object. They demonstrated that a natural consequence is the formation of bipolar outflows and, in particular, they found that for density contrasts between the equator and the poles of 0.1–1 %, the outflow has velocities of 0.1–0.3 times the local escape velocity.

HM Sge might be similar to what has been reported for R Aqr where the jet-like features are spatially resolved in soft X-ray emission by Chandra (Kellogg et al. 2001) which are feeding an even more extended soft region detected by XMM-Newton (Toalá et al. 2022). We note that in the case of HM Sge the XMM-Newton observations do not resolve these jet-like features.

The contribution from the softer component ($E < 0.5$ keV) questions previous classification of HM Sge as a β -type symbiotic stars. It appears that a more accurate classification would be a α/β -type, but we note that such classification has not been suggested in the literature (see, e.g., Merc et al. 2019b, and references therein). Finally, we note that such change in spectral characteristics raise strong questions on the initial classification of those sources that have not been monitored in recent years.

3.2. PU Vul

The EPIC-pn spectrum of PU Vul also seem to display the contribution from emission lines in the 0.2–2.0 keV (see Fig. 1 right panel). One can attribute the dominant peaks in the spectrum to the contribution from N VI 29.54 Å (0.42 keV), N VI 24.78 Å (0.5 keV), and to a lesser extend to those of N VII 19.36 Å (0.64 keV). Some emission at ~ 0.37 keV in the EPIC-pn spectrum might suggest at the presence of C VI 33.7 Å, but this wavelength range is noisy in the RGS spectrum of PU Vul (see Fig. A1 bottom panel). A secondary peak between 0.8–1.0 keV can be attributed to the Fe XVII 16.78 Å (0.74 keV), Fe XVII 15.02 Å (0.83 keV), and Ne X 12.14 Å (1.0 keV) emission lines marginally detected in the RGS spectrum. No considerable emission is detected beyond 2.0 keV.

Single-plasma temperature models did not result in acceptable fits to the EPIC-pn spectrum ($\chi_{\text{DoF}}^2 > 2$). The best fit ($\chi_{\text{DoF}}^2 = 32.99/26 = 1.27$) corresponds to a two-plasma model with typical temperatures of $kT_1 = 0.15$ keV ($= 1.7 \times 10^6$ K) and $kT_2 = 0.75$ keV ($= 8.7 \times 10^6$ K), with the softer component being the dominant one. The total intrinsic X-ray flux and luminosity are $F_X = (8.2 \pm 1.8) \times 10^{-14}$ erg cm $^{-2}$ s $^{-1}$ and $L_X = (1.6 \pm 0.4) \times 10^{32}$ erg s $^{-1}$.

Mürset et al. (1997) obtained a relatively worse model to the ROSAT PSPC data. These authors restricted their study to one-temperature plasma models given the quality of their spectrum. We note that the model presented for PU Vul by Mürset et al. (1997) does not produce a good fit to the observed spectrum (see fig. 3 in that paper). Their dominant plasma temperature ($\sim 6.2 \times 10^6$ K) represents an intermediate value of the temperatures obtained in our best model to the EPIC-pn spectrum. Our luminosity is also consistent (within error bars) with the one reported in Mürset et al. (1997) once considering that those authors used a distance of 1.8 kpc to PU Vul.

The EPIC data of PU Vul presented here confirm this source as a β -type X-ray-emitting symbiotic star (Mürset et al. 1997), where the strong wind from the WD component is slamming the slow wind from the cool component and producing X-ray-emitting gas. We note that a few authors (see

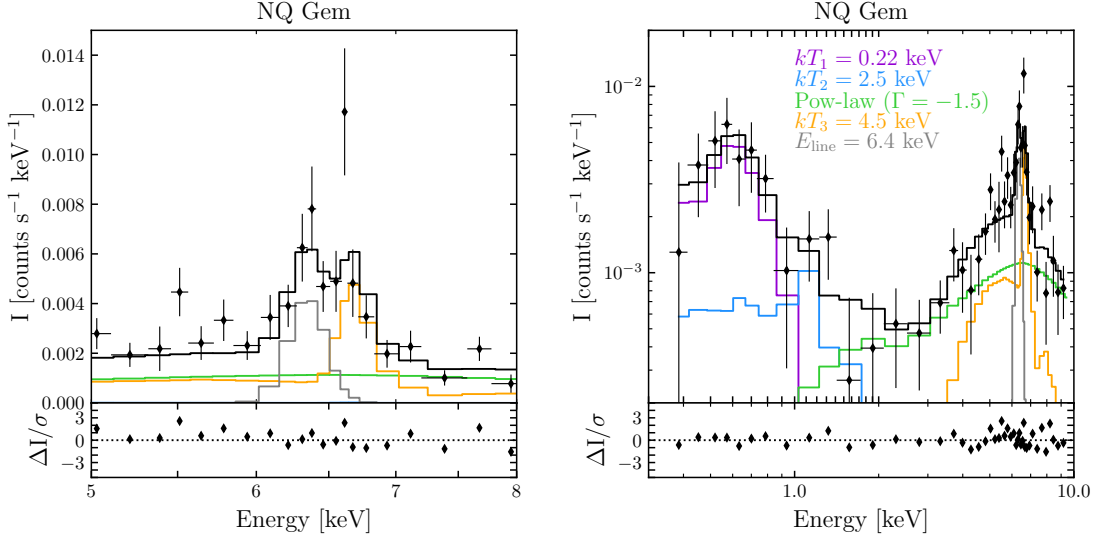


Figure 2. Background-subtracted EPIC-pn spectrum of NQ Gem (black diamonds). Left: Linear scale of the 5.0–8.0 keV energy range showing the Fe emission complex. Right: A log-linear scale of the EPIC-pn spectrum presented in the middle panel of Fig. 1. In both panels the best-fit model to the EPIC-pn spectrum is presented with a black histogram whilst different components are shown in colors (see Table 2 for details). In both cases the bottom panels show the residuals.

for example Nussbaumer & Vogel 1996; Skopal 2006) have reported that the WD component in PU Vul has a stellar wind velocity of about $\gtrsim 1000 \text{ km s}^{-1}$, which can easily produce shocked gas with temperatures of a few times 10^6 K .

3.3. NQ Gem

The EPIC-pn spectrum of NQ Gem discloses a more complicated spectral shape, as previously reported by Luna et al. (2013). These authors classified NQ Gem as a β/δ -type symbiotic star given its clear presence of soft and hard emission in its spectrum. The EPIC-pn spectrum presented in the middle panel of Fig. 1 reveals that the soft emission has a double peak, a broad dominant feature peaking at $\sim 0.55 \text{ keV}$, and a secondary peaking at $\sim 1.2 \text{ keV}$. The broad feature spans from 0.4 to 1.0 keV and seem to be the result of blending from different emission lines detected in the $\sim 13\text{--}30 \text{ \AA}$ wavelength range of the RGS spectrum (see Fig. A1 third panel). The secondary peak seems to include the contribution from emission lines in the $\sim 8\text{--}13 \text{ \AA}$ (Fig. A1 second panel). In the left panel of Fig. 2 we show that the harder emission ($E > 4.0 \text{ keV}$) exhibits the presence of the Fe complex⁶ at $\sim 6.5 \text{ keV}$, the later marginally detected in the Swift data (see fig. 1 in Luna et al. 2013) and typically attributed to the presence of an accretion disk (see, e.g., Eze 2014, and references therein).

Luna et al. (2013) argued that the best fit to the Swift XRT spectrum of NQ Gem includes a slightly-absorbed thermal component ($N_{\text{H},1} \lesssim 10^{21} \text{ cm}^{-2}$, $kT_1=0.23 \text{ keV}$) plus a heavily-absorbed component ($N_{\text{H},2}=90 \times 10^{21} \text{ cm}^{-2}$,

$kT_2 \gtrsim 16 \text{ keV}$). We started our spectral fitting by attempting similar models, but these were not able to appropriately reproduce the 1.0–4.0 keV energy range and did not result in acceptable fits ($\chi_{\text{DoF}}^2 > 2$). In order to fit the secondary peak of the soft emission (that at $\sim 1.2 \text{ keV}$), it was necessary to include of a second *apec* component. However, that model did not result in an acceptable fit either. A subsequent model adding an extra component in order to fit the 2.0–4.0 keV energy range was required. Models including three slightly-absorbed thermal components did not result in acceptable fits. XSPEC was unable to restrict the plasma temperature of the third component, yielding extremely large values. Consequently, the best model ($\chi_{\text{DoF}}^2=36.20/32=1.13$) includes two absorbed temperature models, a power law, and a heavily-absorbed thermal component with extra contribution from a Gaussian in order to fit the Fe emission. That is,

$$N_{\text{H},1} \times (\text{apec}_1 + \text{apec}_2 + \text{pow}) + N_{\text{H},2} \times (\text{apec}_3 + \text{Gauss}). \quad (1)$$

Here the Gaussian component is needed to fit the 6.4 keV emission line. The parameters used in XSPEC to perform a fit using a Gaussian profile are the line energy E_{line} , the line width (σ_{line}) in keV, and normalization parameter (A_{line}).

The soft energy range of the EPIC-pn spectrum ($E < 4.0 \text{ keV}$) is reproduced by the contribution from plasma components with temperatures of $kT_1=0.22 \text{ keV}$ and $kT_2=0.31 \text{ keV}$ in addition to a power law with a photon index of $\Gamma = -1.25$ that also contributes to the harder spectral region (see Fig. 2 right panel). The heavily-absorbed component has an hydrogen column density of $N_{\text{H},2} = 3.9 \times 10^{23} \text{ cm}^{-2}$ with a plasma temperature of $kT_3=4.5 \text{ keV}$. This component also produces the contribution from the He-like component of the Fe emission line at 6.7 keV (orange

⁶ This complex is composed by the fluorescent, He-like and H-like Fe lines at 6.4, 6.7 and 6.9 keV.

line in Fig. 2). The total intrinsic X-ray flux and luminosity of this model are $F_X=(2.7\pm 0.5)\times 10^{-13}$ erg cm $^{-2}$ s $^{-1}$ and $L_X=(3.4\pm 0.6)\times 10^{31}$ erg s $^{-1}$, respectively. These values are slightly smaller than those presented by Luna et al. (2013).

X-ray spectral modeling of β/δ -type symbiotic stars is usually attempted with simpler models as that presented here. But the higher quality EPIC-pn spectrum of NQ Gem suggests that some extra components are to be taken into account to appropriately fit the 1.0–4.0 keV energy range. We note that the power law component (usually associated with non-thermal emission) might not be the best option to assess the physics behind the production of X-rays in NQ Gem. The power law component improves the goodness of the fit, but it might suggest the need of a continuous distribution of temperatures.

This situation might be the same for other other β/δ -type symbiotic stars, such is the case of CH Cyg. For example, Mukai et al. (2007) presented Suzaku observations of CH Cyg and used a two-plasma components fits to model the XIS spectra. Their figure 1 shows that the 2.0–4.0 keV energy range is not very well fitted by the proposed model. The analysis of archival XMM-Newton observations of CH Cyg suggest that another approach to fit this energy range is to include the presence of a reflection component (Ishida et al. 2009) very similar to that used for active galactic nuclei (Toalá et al. in prep.). A subsequent study of high-quality observations of β/δ -type symbiotic stars will help understanding accretion processes and the effects of reflection behind the production of X-rays.

4. SUMMARY

We presented the analysis of archival XMM-Newton observations of three symbiotic stars, namely, HM Sge, NQ Gem, and PU Vul. In the three cases, their EPIC-pn spectra have higher-quality than previous spectra presented in the literature. The EPIC-pn spectra hint at the presence of emission lines that is further corroborated by the RGS spectra of the three sources. The analysis of these sources improves previous determination of their X-ray properties, but the determination of fluxes and luminosities agree with previous works. Our findings can be summarized as follows:

- **HM Sge.** We detected an extra soft component in the EPIC-pn spectrum of HM Sge not detected by ROSAT, similarly to what is found for α -type symbiotic stars. This corresponds to a plasma with temperature of 2.9×10^{-2} keV ($=3.4\times 10^5$ K). Although α -type symbiotic stars are associated with thermonuclear

burning on the surface of the WD component, we suggest that in the case of HM Sge it might be attributed to the action of jets with velocities of $\gtrsim 100$ km s $^{-1}$. We suggest a spectral classification of α/β which is an new alternative to the one proposed before.

- **PU Vul.** The model that best reproduces the EPIC-pn spectrum of PU Vul includes the contribution from two thermal plasma components, 0.22 keV ($=1.7\times 10^6$ K) and 0.75 keV ($=8.7\times 10^6$ K). We confirm that this symbiotic star can be classified as a β -type.
- **NQ Gem.** The EPIC-pn spectrum of this β/δ -type symbiotic star unambiguously exhibits the presence of the Fe emission lines above 6.0 keV. Two-temperature plasma models, which are typically used to fit the spectrum of this class of symbiotic star, fail to reproduce the EPIC-pn spectrum of NQ Gem. The model requires at least two extra components in order to fit the 1.0–4.0 keV energy range: an extra optically-thin plasma and a power law component. We suggest that the power law component, usually associated with non-thermal emission does not represent the true nature of the X-ray emission in this source. Alternatively, we suggest that more sophisticated models including reflection components should be used to model β/δ -type symbiotic stars.

The authors thank comments and suggestions from an anonymous referee that helped improving the presentation and interpretation of the results. J.A.T. thanks Fundación Marcos Moshinsky (Mexico) and the UNAM PAPIIT project IA101622. M.K.B. thanks Consejo Nacional de Ciencias y Tecnología (CONACyT, Mexico) for research student grant. L.S. and M.K.B. also acknowledge support from UNAM PAPIIT project IN110122. This work is based on observations obtained with XMM-Newton, an European Science Agency (ESA) science mission with instruments and contributions directly funded by ESA Member States and NASA. This work has made extensive use of NASA’s Astrophysics Data System.

Facilities: XMM-Newton (EPIC)

Software: SAS (Gabriel et al. 2004), XSPEC (Arnaud 1996)

APPENDIX

A. RGS SPECTRA

The RGS spectra of the three symbiotic stars analyzed here were processed using the SAS tasks *rgsproc*. This task produces source and background spectra as well as the necessary calibration matrices. First order spectra were extracted from

the RGS1 and RGS2 instruments and were then combined using the SAS task *rgscombine*.

In Fig. A1 we present the background-subtracted 1st order RGS(1+2) spectra of HM Sge, NQ Gem, and PU Vul. The RGS spectra cover the 5–38 Å wavelength range which

corresponds to the $\sim 0.32\text{--}2.48$ keV energy range. The most prominent emission lines are labeled on each spectrum. Although shallow, these spectra confirm that the peaks in the

EPIC-pn spectrum can be related to the presence of emission lines. A detailed analysis of RGS spectra of a sample of symbiotic stars will be presented in a separate work.

REFERENCES

- Aguayo-Ortiz, A., Tejada, E., & Hernandez, X. 2019, *MNRAS*, 490, 5078
- Aizu, K. 1973, *Progress of Theoretical Physics*, 49, 1184
- Akras, S., Guzman-Ramirez, L., Leal-Ferreira, M. L., et al. 2019, *ApJS*, 240, 21
- Arnaud, K. A. 1996, *Astronomical Data Analysis Software and Systems V*, 101, 17
- Bailer-Jones, C. A. L., Rybizki, J., Fouesneau, M., et al. 2021, *AJ*, 161, 147
- Bondi, H. & Hoyle, F. 1944, *MNRAS*, 104, 273
- Chakrabarty, D. & Roche, P. 1997, *ApJ*, 489, 254
- Chernyakova, M., Courvoisier, T. J.-L., Rodriguez, J., et al. 2005, *The Astronomer's Telegram*, 519
- Corradi, R. L. M., Ferrer, O. E., Schwarz, H. E., et al. 1999, *A&A*, 348, 978
- Dickey, J. M. & Lockman, F. J. 1990, *ARA&A*, 28, 215
- Enoto, T., Sasano, M., Yamada, S., et al. 2014, *ApJ*, 786, 127
- Eze, R. N. C. 2014, *MNRAS*, 437, 857. doi:10.1093/mnras/stt1947
- Gabriel, C., Denby, M., Fyfe, D. J., et al. 2004, *Astronomical Data Analysis Software and Systems (ADASS) XIII*, 314, 759
- Goldman, S. R., Sankrit, R., Wolthuis, N., et al. 2022, *Research Notes of the American Astronomical Society*, 6, 159
- HI4PI Collaboration, Ben Bekhti, N., Flöer, L., et al. 2016, *A&A*, 594, A116
- Hinkle, K. H., Fekel, F. C., Joyce, R. R., et al. 2019, *ApJ*, 872, 43
- Ishida, M., Okada, S., Hayashi, T., et al. 2009, *PASJ*, 61, S77
- Kalberla, P. M. W., Burton, W. B., Hartmann, D., et al. 2005, *A&A*, 440, 775
- Karovska, M., Gaetz, T. J., Carilli, C. L., et al. 2010, *ApJL*, 710, L132
- Kellogg, E., Pedelty, J. A., & Lyon, R. G. 2001, *ApJL*, 563, L151
- Kennea, J. A., Mukai, K., Sokoloski, J. L., et al. 2009, *ApJ*, 701, 1992
- Lodders, K., Palme, H., & Gail, H.-P. 2009, *Landolt & Bornstein*, 4B, 712
- Luna, G. J. M., Sokoloski, J. L., Mukai, K., et al. 2013, *A&A*, 559, A6
- Merc, J., Gális, R., & Wolf, M. 2019, *Research Notes of the American Astronomical Society*, 3, 28
- Merc, J., Gális, R., & Wolf, M. 2019, *Astronomische Nachrichten*, 340, 598
- Montez, R., Luna, G. J. M., Mukai, K., et al. 2022, *ApJ*, 926, 100
- Mukai, K. 2017, *PASP*, 129, 062001
- Mukai, K., Ishida, M., Kilbourne, C., et al. 2007, *PASJ*, 59, 177
- Mürset, U., Wolff, B., & Jordan, S. 1997, *A&A*, 319, 201
- Nussbaumer, H. & Vogel, M. 1996, *A&A*, 307, 470
- Orio, M., Zezas, A., Munari, U., et al. 2007, *ApJ*, 661, 1105
- Podsiadlowski, P. & Mohamed, S. 2007, *Baltic Astronomy*, 16, 26
- Skopal, A. 2006, *A&A*, 457, 1003
- Toalá, J. A., Sabin, L., Guerrero, M. A., et al. 2022, *ApJL*, 927, L20
- Wilms, J., Allen, A., & McCray, R. 2000, *ApJ*, 542, 914

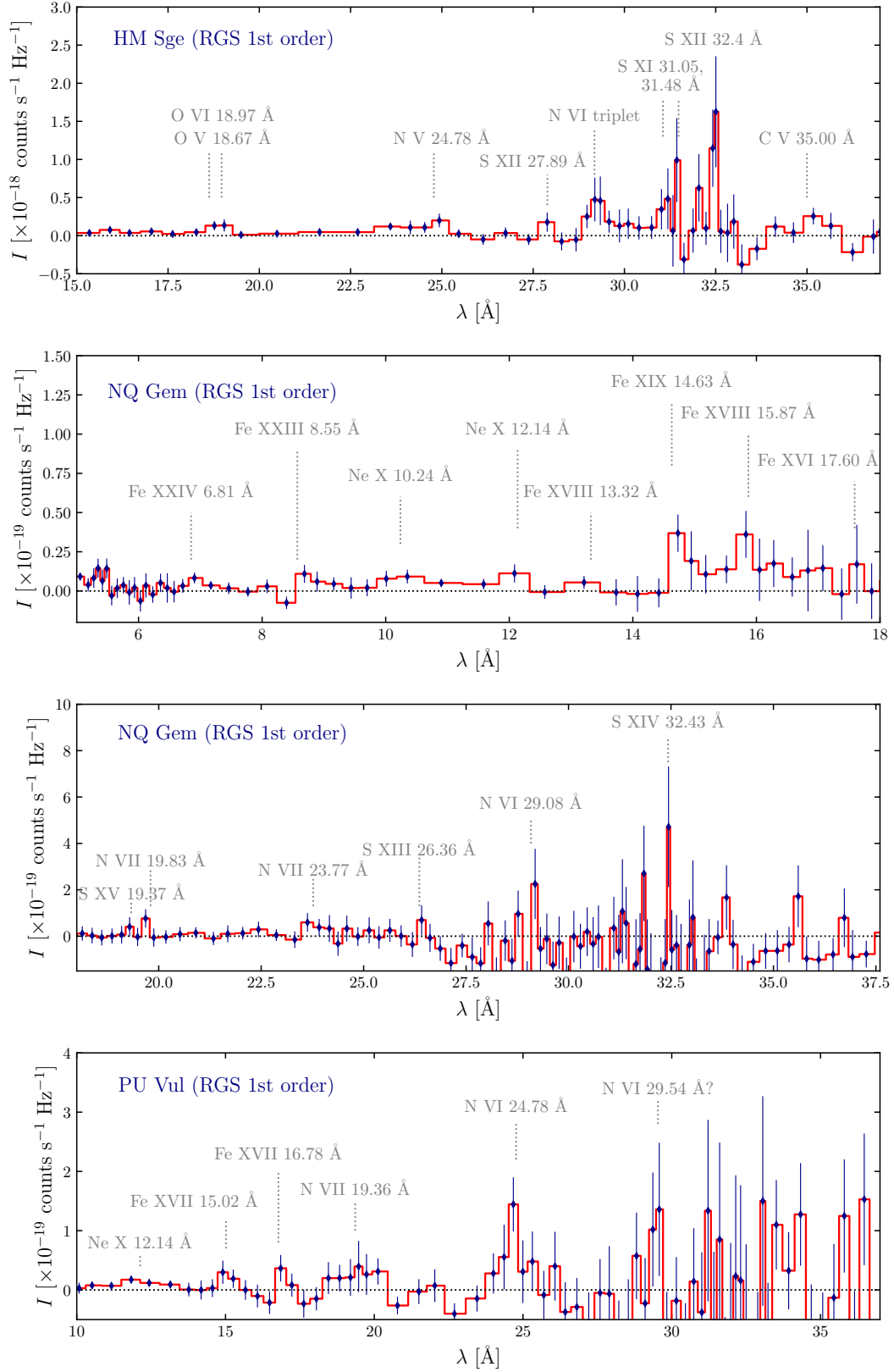


Figure A1. 1st order RGS(1+2) spectra of HM Sge (first panel), NQ Gem (second and third panels), and PU Vul (bottom panel). The most prominent lines are labeled.